Highly-dispersed ultrafine Pt nanoparticles on microemulsion-mediated TiO2 for production of hydrogen and valuable chemicals via oxidative photo-dehydrogenation of glycerol

Valeriia Maslova, Elsje Alessandra Quadrelli, Pooja Gaval, Andrea Fasolini, Stefania Albonetti, Francesco Basile

Highly-dispersed ultrafine Pt nanoparticles on microemulsion-mediated TiO_2 for production of hydrogen and valuable chemicals via oxidative photo-dehydrogenation of glycerol

Valeriia Maslova [a,b], Elsje Alessandra Quadrelli [b,*,1], Pooja Gaval [a,b], Andrea Fasolini [a], Stefania Albonetti [a,*], Francesco Basile [a,*]

[a] *Dip. Chimica Industriale "Toso Montanari", Università di Bologna, Viale Risorgimento 4, 40136 Bologna (BO), Italy*
[b] *Université de Lyon, C2P2 (UMR 5265 CNRS, Université de Lyon 1, CPE Lyon), France*

The oxidative photo-dehydrogenation of glycerol to produce H_2 and other valuable chemicals was studied using different materials. In particular, Pt nanoparticles were deposited on microemulsion-synthesized TiO_2 via surface organometallic chemistry (SOMC) and compared with photocatalysts obtained using more conventional methods. Well-defined Pt(II) single-site titania-grafted were prepared reacting the surface hydroxyl groups of TiO_2 nano-oxides with the organometallic $Pt(COD)Me_2$ complex. Sample reduction under H_2 generated ultrafine Pt nanoparticles well-dispersed on titania surface. Its performance under simulated solar light showed superior activity when compared to analogous Pt-containing catalysts prepared by other methods. Improved dispersion of Pt metal on titania surface was among the primary reasons of a better overall activity, providing relatively high rates of hydrogen productivity. Moreover, an increase of glyceraldehyde productivity in liquid phase was observed with the increase of Pt dispersion, demonstrating that the metal dispersion can strongly affect the selectivity of chemicals produced in the reaction. Comparison with state of the art shows that the present ma-terial exhibits excellent performance for a combined positive effect of the high specific surface area of titania prepared by microemulsion, giving access to the increased densities of active sites and the high dispersion of Pt nanoparticles given by the SOMC technique.

1. Introduction

The use of renewable energy, adoption of biomass as feedstock and new technologies for energy production are among the sustainability megatrends [1]. In this view, glycerol, a cheap and renewable biomass feedstock, co-product of triglyceride transesterification, which amounts to ca. 10 kg (with purity of 50–55%) per 100 kg of biodiesel produced [2], is considered a chemical platform molecule with high potential. Glycerol is used as substrate in thermo-, electro-, and photo-reforming processes involving hydrogenolysis, dehydration, esterification, etherification, oligomerization, polymerization, carbonylation, and oxidation reactions [3], and produces a variety of high added-value chemicals for the agrochemical and polymer industry, which can also be used as solvents, surfactants, adhesives, coatings and building blocks for other compounds [4]. The production of hydrogen from glycerol is among these high potential routes. It is expected for example, inter alia, to increase the profitability of biodiesel production [3,5].

Both steam reforming and aqueous phase reforming of glycerol lead to hydrogen production [6,7], but high energy consumption and operating costs are required due to the endothermic character of these processes. Heterogeneous photocatalysis can be thus regarded as an interesting alternative, energy saving way of glycerol valorization in the context of sustainability. The process of photoreforming of oxygenated substrates in anaerobic conditions to yield H_2 and CO_2 using suspension of semiconductor-based photocatalysts has been extensively studied [8,9]. Among the semiconductors thermodynamically capable of glycerol photoreforming, such as oxides [10–17], metallates [18,19], sulfides [20,21], different composites [15,22–29] etc., TiO_2 has drawn the greatest attention, because it is a cheap, non-toxic, abundant material with a good thermal and photo-stability. The addition of a metal in the

* Corresponding authors
E-mail addresses: quadrelli@cpe.fr (E.A. Quadrelli), stefania.albonetti@unibo.it (S. Albonetti), f.basile@unibo.it (F. Basile).
[1] Present address: Université de Lyon, CNRS IRCELYON (UMR 5256, Université Claude Bernard Lyon 1), 2 Avenue Albert Einstein, 69626 Villeurbanne, France.

form of nanoparticles helps to enhance hydrogen production as they serve as co-catalyst for proton reduction reaction. In the last ten years [30] several metals have been used as titania dopants for glycerol photoreforming (e.g. Pt [11,31–35], Au [31,34,35] Pd [31,35–37], Ni [38], Cu [39]). Among these, Pt nanoparticles (NPs) showed the best results because of a greater work function of this metal [35,40] and the possibility to synthesize small clusters of around 1 nm, which display a high dispersion [9]. Nevertheless, Pt dispersion can be affected by the synthetic route employed for both support and Pt NPs, and interaction between them.

Surface organometallic chemistry (SOMC) is an established technique allowing synthesizing a heterogeneous catalyst with well-defined active sites by reacting in a controlled fashion the organometallic and coordination complexes with the molecularly-identified reactive surface sites of the support, typically a solid oxide. This approach allows in the best cases a structure-activity relationship as in homogeneous catalysis [41] and can lead to performing catalysts [42–45]. Recently, metal and metal oxide nanoparticles prepared by using different SOMC approaches [46–48] have been applied in catalytic reactions, e.g. soot oxidation [49–51], hydrogenation of toluene [52], dehydrogenation of isobutene and CO oxidation [53], styrene hydrogenation [54], alkene hydrosilylation [55]. Beneficial effect of Rh clusters in methane hydrogenolysis was observed for pre-grafted $Rh(\eta^3\text{-}C_3H_5)_3$ on TiO_2 and subsequently reduced in hydrogen compared to the sample prepared by incipient impregnation [46]. Nonetheless, in the field of photocatalysis the use of photo-active materials prepared by SOMC is rarely described. Preparation of single-atom cobalt centers on different supports and its testing in photocatalytic water splitting was reported by H. Ahn and co-workers [56]. Recently, Jeantelot et al. [57,58] reported superior activity of isolated Pt atoms on TiO_2 and ultrafine Pt on $SrTiO_3$ using Pt(COD)Me_2 organometallic precursor in photocatalytic water splitting with methanol as sacrificing agent compared to Pt-containing materials prepared by impregnation method.

In present work, titanium dioxide was synthesized in the form of nano-powder using a microemulsion-mediated system. The synthesis delivered high surface area anatase TiO_2 polymorph with a small amount of rutile. XRD and DRIFT analyses were used to select the appropriate temperature for dehydroxylation process, which allows generation of well-defined sites on the surface of TiO_2, in principle hydroxyls, capable for grafting of Pt precursor complex. The reduction of grafted Pt(COD)Me_2 organometallic complex on the surface of synthesized titania resulted in well-dispersed ultrafine Pt nanoparticles and provided higher dispersion than classical incipient wetness impregnation and deposition precipitation methods. The photo-catalytic activity of these samples in the glycerol oxidative photo-dehydrogenation process towards hydrogen evolution as well as production of liquid phase products were tested and compared.

2. Experimental

2.1. Catalyst preparation

TiO_2 nano-oxides were prepared by reverse microemulsion method based on the modification of procedure reported by Andersson et al. [59], by breaking the microemulsion through heating under reflux. The modifications were introduced also in composition of microemulsion as follows: titania precursor was dissolved in organic instead of aqueous phase, water-to-surfactant molar ratio was equal to 21.29. In brief, the oil phase composed by cyclohexane (99%, Alfa Aesar), dispersant, Triton X-100 (Alfa Aesar), surfactant, and n-hexanol (99%, Alfa Aesar), co-surfactant, was mixed with 5 M aqueous solution of HNO_3 (65%, Sigma Aldrich), forming transparent system of microemulsion. Another oil phase was prepared adding titania precursor, titanium (IV) butoxide (97%, Sigma Aldrich). After stirring until being transparent, this solution was added to previously prepared microemulsion under vigorous stirring. The resulting reverse microemulsion system was stirred for 1 h at room temperature, and then heated up to 74 °C under reflux and kept for 5 h under vigorous stirring. The resulting solid was separated by centrifugation and washed with ethanol (99.8%, Sigma Aldrich) 5 times. The obtained paste was dried overnight at 100 °C and calcined at 400 °C for 3 h with the ramp of 2 °C/min. Resulting solid powder is denominated as **TiO_2-m**.

Physisorbed layers of water were removed by treatment under dynamic vacuum as follow: 1 g of catalyst **TiO_2-m** was placed either in a 30 cm glass reactor and heated up to the target temperature (200 °C or 500 °C) or in a quartz reactor to reach 700 °C with the rate of 3 °C/min for 12 h under dynamic vacuum (10–5 mbar). Samples were transferred in a glovebox, and stored under argon. This dehydroxylated samples are called **TiO_2-m-T** (T = 200, 500 and 700, respectively).

Grafting of Pt(COD)Me_2 over **TiO_2-m-500** surface was performed as follow: the powder **TiO_2-m-500** (758.7 mg) was placed in a double Schlenk flask in glovebox. Dimethyl(cyclooctadiene)platinum (19.5 mg, 0.058 mmol, Alfa Aesar) was placed in the second reactor of the double Schlenk flask inside the glovebox. The amount of Pt(COD)Me_2 was chosen to achieve the nominal loading of 1.5%wt, a common value in the literature for photo-reforming essays. Degassed and dried pentane (5 ml) was added under argon atmosphere to the platinum complex and the solution was then transferred onto powder. The reaction was kept for 2 h under stirring at room temperature. The gaseous products of reaction as well as solvent were transferred into 6 L glass balloon for GC and GC-MS analysis. The resulting solid **Pt-OM@TiO_2-m-500** was dried under dynamic vacuum at room temperature overnight and stored in a glovebox.

Solid **Pt-OM@TiO_2-m-500** (400.4 mg) was transferred to 500 ml glass reactor and exposed to H_2 (450 mbar) at 300 °C (5 °C/min) for 3 h to yield the Pt NP-loaded sampled obtained from the organometallic route, named **Pt/TiO_2-m_SOMC**.

For comparison of preparation methods of Pt NPs and their effect on catalyst activity, two other samples were obtained by incipient wetness impregnation (IWI) and deposition-precipitation (DP) methods. For the IWI procedure, aqueous solution of $H_2PtCl_6 \cdot x\ H_2O$ (0.1868 M, 870 μl, 99.99%, Alfa Aesar, Premion®) was loaded on **TiO_2-m** powder (2 g), followed by drying in oven at 100 °C. Finally, the powder was dried at 120 °C overnight, calcined at 350 °C for 3 h (ramp 10 °C/min) in static air and sieved with 60–80 mesh. The powder was exposed to H_2/N_2 flow (100 ml/min, 10%) at 350 °C for 3 h (ramp 10 °C/min) in static air, to yield material **Pt/TiO_2-m_IWI**. The DP synthesis was performed as follow: an aqueous solution of $[Pt(NH_3)_4](NO_3)_2$ (0.001 M, 0.117 ml, 99.9%, Alfa Aesar) was used at pH 8, adjusted by adding dropwise a 0.1 M NaOH solution. The resulting solution was added dropwise to the **TiO_2-m** suspension (1.5 g) in water (150 ml) under vigorous stirring at room temperature with a dropwise addition of 0.1 M NaOH to maintain pH 8. Once the entire platinum solution was transferred to the **TiO_2-m** suspension, the temperature was increased to 65 °C, and the suspension was stirred for 2 h. The solid was then separated by centrifugation, washed several times with water, dried at 110 °C overnight and calcined at 350 °C for 3 h with a rate of 10 °C/min) in static air and sieved with 60–80 mesh. The material (light gray powder, 1 g) was exposed to H_2/He flow (100 ml/min, 5%) at 350 °C for 3 h (ramp 10 °C/min). The resulting catalyst was denoted **Pt/TiO_2-m_DP**. All the platinum-containing titania-based solids had a nominal loading in platinum of 1.5 wt%. The actual loading was determined by elemental analysis and is reported in Table 1.

2.2. Catalyst characterization

The prepared materials were characterized in terms of their specific surface area, phase composition and light absorption properties, using nitrogen physisorption at the temperature of liquid nitrogen, X-ray diffraction (XRD), and diffuse reflectance UV–vis spectroscopy (DRS).

Nitrogen adsorption desorption isotherms were measured on Belsorp-Max from BEL-JAPAN at 77 K after degassing the sample. No

Table 1
Data on specific surface area (S_{BET}), crystalline size of titania (d_{TiO2}), mean size of Pt (d_{Pt}), dispersion of Pt (FE), energy bandgap (E_g), elemental analysis represented in units of mass percent (wt%).

Sample name	S_{BET} (m^2/g)	d_{TiO2} (nm)	d_{Pt}[a] (nm)	FE[b]	Element	wt %	E_g[c] (eV)
Pt-OM@TiO_2-m-500	121	–	–	–	C Pt	0.97 1.22	–
Pt/TiO_2-m-SOMC	100	9	1.01	0.87	–	–	3.12
Pt/TiO_2-m_DP	128	7	0.93	0.31	Pt	1.22	3.11
Pt/TiO_2-m_IWI	121	8	1.87	0.11	Pt	1.40	3.11

[a] Particle size of platinum determined from TEM analysis for reduced samples.
[b] Pt dispersion calculated following A. Borodziński et al. [75] (see SI for more information).
[c] Energy bandgap of reduced samples estimated from Kubelka-Munk spectra.

heat-pretreatment was performed on dehydroxylated samples (**TiO_2-m-200**, **TiO_2-m-500**, **TiO_2-m-700**, **Pt-OM@TiO_2-m-500**) stored in the glove box. The samples prepared and stored in air (namely **TiO_2-m**, **Pt/TiO_2-m_DP**, **Pt/TiO_2-m_IWI**) were pre-treated at 125 °C for 2 h prior nitrogen adsorption. The specific surface area of the sample powder was calculated according to the BET model, BJH method was used to calculate the pore size.

Powder X-ray diffraction analyses of **TiO_2-m**, **TiO_2-m-200**, **TiO_2-m-500**, **TiO_2-m-700** samples were performed using Bruker D8 Advance instrument (Cu, Kα radiation, λ = 1.5406 Å, 40 kV, 4 MA). A thin smooth layer of the sample was deposited by evaporation from a suspension in ethanol on a non-crystalline substrate such as poly(methyl methacrylate). The XRD patterns were recorded from 5° to 70° at a step of 0.02° 2θ. The XRD of samples **Pt/TiO2-m_A_SOMC**, **Pt/TiO_2_IWI** and **Pt/TiO_2_DP** were carried out at room temperature with a Bragg/Brentano diffractometer (X'pertPro PANalytical) equipped with a fast X'Celerator detector, using a Cu anode as the X-ray source (Kα, λ = 1.5418 Å). Diffractograms were recorded in the range of 10–80°2θ with a step of 0.05°2θ. Particle size was determined by Scherrer equation over the 100% peak.

Diffuse reflectance UV–vis spectroscopy analyses were carried out in a Perkin Elmer Lambda 19 instrument equipped with integrating sphere in the range 280–800 nm. Diffuse Reflectance Infrared **Fourier Transform (DRIFT) spectra** were recorded on a Nicolet 6700-FT spectrometer using a cell equipped with CaF_2 window. DRIFT spectra were treated through Kubelka-Munk function (KM). **Elemental analyses** of C and Pt content were performed using CH-analyzer (Heraeus/Mannertz/Mikroanalytisches Labor Pascher) instrument and inductively coupled plasma (ICP) atomic emission spectrometer iCap 6500 (Thermo Fisher Scientific) at the Mikroanalytisches Labor Pascher in Remagen-Bandorf, Germany.

Solid state NMR spectra were collected on BRUKER AVANCE III 500 spectrometer operating at 125 MHz for 13 C. The zirconia rotor of 4 mm was filled with the desired product inside glove box under argon and sealed with a kel-f stopper. It was then transferred into the probe Bruker CP 4 mm spectrometer allowing rotation of the rotor at a speed of 10 kHz. The time between two acquisitions was always optimized to allow complete relaxation of the protons.

Transmission electron microscopy (TEM) analysis of **Pt/TiO_2-m_SOMC** was performed using a JEOL 2100F electron microscope at the "Centre Technologique des Microstructures", Université Claude Bernard Lyon 1, Villeurbanne, France. The acceleration voltage was 200 kV. The samples were prepared by dispersing a drop of the ethanol suspension of a ground sample on a Cu grid covered by a carbon film. Whereas, TEM images of the samples **Pt/TiO_2-m_IWI** and **Pt/TiO_2-m_DP** were done at IMM_CNR, Bologna, Italy. The analyses were carried out using TEM/STEM FEI TECNAI F20 instrument, equipped with a high-angle annular dark field (HAADF) detector at 200 keV. The corresponding samples were suspended in ethanol and treated in ultrasonic bath for 15 min. The suspension was deposited on a "quantifoil carbon film" Cu grid for TEM analysis, then dried at 100 °C.

2.3. Photocatalytic test and analytical methods

Prepared materials were tested in oxidative photo-dehydrogenation of glycerol in a sealed top-irradiated glass photo-reactor (Fig. S1). Prior the reaction, 1 M, 21.5 ml aqueous solution of glycerol with 0.5 g/L of catalyst were stirred for 20 min in the dark, while purging continuously N_2. The amount of catalyst was optimized following Kisch [60]. The sealed reactor with inner diameter of 4.6 cm was irradiated for 6 h using the solar simulator that consists of 300 W Xe lamp (irradiance of 100 mW/cm^2 was regularly measured prior each test by radiometer HD2102.2 DELTA OHM equipped with two probes of 315–400 nm and 400–1050 nm). Samples were collected at the end of the reaction. After reaction, the samples were qualitatively analyzed by Electrospray Ionization Mass-spectrometry (ESI-MS) and Nuclear Magnetic Resonance (NMR) techniques for identification of the products. Waters micromass ZQ 4000 instrument with quadrupole mass analyzer was used to perform ESI-MS analysis. The aqueous product solution was diluted in methanol and injected without further derivatization. Positive ions conditions were 3.53 kV for the probe and 10 V for the cone, while for negative ions the probe voltage was 2.54 kV and 40 V for the cone with a 20 μl/min flux. 600 MHz ^{1}H NMR analysis was performed using Varian Inova (600 MHz for 1 H) equipped with an indirect triple resonance probe. The data treatment was done using a presaturation sequence (PRESAT, with power = 4 dB and presaturation delay 2 s), while analyzing aqueous solutions (the residual H_2O signal δ 4.79 ppm). After the reaction, the liquid phase was filtered, diluted 100 times (from 1 M to 0.01 M) and analyzed in an Agilent HPLC over Rezex ROA Organic Acid column (0.0025 M H_2SO_4 eluent, oven temperature 30 °C and 0.6 ml/min flux) with DAD and RID detectors. Aqueous solutions of commercial standards were used to calibrate the products by external method. Hydrogen was analyzed in off-line Agilent Technologies GC equipped with CP Molesieve 5 A UM 25 m × 0.53 mm × 50 μm column and TCD detector. The calibration was performed using constant volume (1 ml) of gas-tight syringe with different molar fractions of H_2/N_2. The other gas phase products were analyzed off-line by Autosystem XL GC with CARBOXENE 1000 60–80 mesh column and flame ionization detector, equipped with methanizer. The calibration was performed injecting different volumes of the commercial mixture of gases with constant molar fraction. The conversion of glycerol and the selectivity (*S*) of products were calculated as follows:

$$Conversion(\%) = \frac{\sum n(product), mol \cdot SF}{n(glycerol)_{in}, mol} \times 100\%$$

$$S\% = \frac{n(product), mol \cdot SF}{\sum n(product), mol \cdot SF} \times 100\%$$

where $n(glycerol)_{in}$ is the initial moles of glycerol, *SF* is the stoichiometry factor, which is equal to 1 for glyceraldehyde, 2/3 for glycolaldehyde and 1/4 for H_2; n is moles of corresponding product.

The solution obtained after the tests were analysed with an Agilent Technologies 4210 MP-AES Inductively Coupled Plasma (ICP) instrument. The analyses showed the absence of Pt in solution, assessing the absence of leaching of the active phase.

3. Results and discussions

3.1. TiO_2 catalysts characterization

The titania obtained by microemulsion, **TiO_2-m**, was mainly

characterized as anatase crystalline polymorph with a small amount of rutile as can be seen from XRD patterns shown on Fig. S2 and Table S1. The crystallite size of **TiO_2-m** was found to be 8 nm with respect to anatase (101) reflection. This is an advantage of microemulsion method, which allows to obtain small crystallites with high surface area together with a control over the composition and morphology of the system compared to other techniques [61–63].

Thermal pre-treatment was carried out under vacuum at different temperatures in order to monitor the transformation of titania, and the presence and amount of isolated hydroxyl groups on the surface since they are considered as primary grafting sites for metal precursor.

After pretreatment at 200 °C (**TiO_2-m-200**) XRD analyses (Fig. S2) showed phase composition and crystallite size similar to the starting material, **TiO_2-m**. At 500 °C the phase composition remained unchanged, although a slight growth of particles was observed in **TiO_2-m-500** due to sintering. Following the 700 °C thermal treatment, the particles size and rutile fraction increased drastically in **TiO_2-m-700** as shown in Fig. S2 (d), resulting in shrinking of surface area, while the pore size increased (Table S1). This is in agreement with the previous literature [64,65] where small anatase particles tended to agglomerate in temperature range above 700 °C due to sintering. This led to the formation of big crystals of rutile, changing the porosity from inter-crystallite pores to inter-agglomerate ones.

DRIFT spectra reported in Fig. S3 provide information about adsorbed species and the presence of hydroxyl groups. The spectra show numerous bands above 3000 cm^{-1} corresponding mainly to physisorbed water, chemisorbed water and surface titanols, Ti-OH [66–69]. While the distinct assignment of each band is beyond the scope of this work, it can be seen that: (*i)* physisorbed water, characterized by very broad bands below 3300 cm^{-1} can be substantially reduced through thermal pre-treatment, as observed starting at 200 °C; at the same time (ii) most of the strongly chemisorbed water, as testified inter alia, by the broad band around 3400 cm^{-1} requires thermal treatment beyond 500 °C to be substantially removed from the surface.

The peaks of a weak intensity that appeared around 2220 cm^{-1} especially after dehydroxylation at 500 °C (Fig. S3) could be assigned to N-containing species [70–72] such as isocyanate groups (-NCO) or cyanate (-CN), whose presence is justified taking into account that in the microemulsion-mediated synthesis of **TiO_2-m** aqueous solution of nitric acid was used as hydrolyzing agent.

Strongly physisorbed CO_2 in the range of 2460 and 2250 cm^{-1} (Fig. S4) indicates the presence of basic sites on **TiO_2-m** and **TiO_2-m-T**. Interestingly, Yamakawa and co-workers [73] reported different frequencies attributed to CO_2 adsorbed at different sites of TiO_2. For instance, the peak at 2340 cm^{-1} was assigned to defective sites related to oxygen vacancies (V_os), which in fact play an important role in photocatalysis, affecting the energy bandgap of the semiconductor. To note, after dehydroxylation process, samples changed color to grayish-blue depending on the temperature, indicating the formation of oxygen deficient sites. On the other hand, the peak at 2350 cm^{-1} was associated with CO_2 adsorbed at the fivefold Ti^{4+} sites of anatase [73]. After dehydroxylation at 700 °C, a peak at 2361 cm^{-1} appeared due to stretching of CO_2 adsorbed at Ti_{5c} on rutile (110) [74]. The presence of rutile is in agreement with the results given by XRD analysis.

In summary, dehydroxylation process removed most physisorbed water from **TiO_2-m**, giving access to non-mobile grafting sites (chemisorbed water and/or surface titanols) on the surface of titania by SOMC technique [43]. For grafting process, **TiO_2-m-500** sample was selected as a compromise between desired crystalline polymorph, namely anatase, and the presence of sizable amount of surface reactive site for further functionalization.

3.2. Pt/TiO2 catalysts preparation and characterization

To examine whether a deposition method can affect the size and dispersion of Pt nanoparticles and, therefore, photocatalytic activity, three different synthetic techniques were used, viz. (i) incipient wetness impregnation, (ii) deposition-precipitation and (iii) grafting of Pt complex via surface organometallic chemistry (SOMC) route. Nominal loading of Pt over titania for all prepared sample was 1.5 wt%. Detailed characterizations are summarized in Table 1.

Grafting of $Pt(COD)Me_2$ over **TiO_2-m-500** surface by SOMC technique was performed in a double Schlenk flask under argon atmosphere at room temperature.

The deposition of Pt precursor on solid **Pt-OM@TiO_2-m-500** was monitored by DRIFT, solid state NMR techniques as well as elemental analysis.

DRIFT spectra on Fig. S5 show disappearance of surface titanols and appearance of peaks around 3018 cm^{-1} and 2950–2850 cm^{-1} that correspond to alkenyl and alkyl C-H stretching of cyclooctadiene and/or methyl of the Pt precursor.

The GC and GC-MS analyses of the gaseous products released during the grafting of $Pt(COD)Me_2$ over **TiO_2-m-500** showed exclusively CH_4, which is in good agreement with reported literature [47,52,57], supporting the formation of monopodal [-O-Pt(COD)Me] and/or bipodal [-O-Pt(COD)-O-] species as shown in Scheme 1.

Elemental analysis (Table 1) showed 1.22 wt% of platinum content for **Pt-OM@TiO_2-m-500**, demonstrating that substantial amount (around 90%) of the organometallic complex dissolved in solution has been grafted. Solid-state $^{13}C\{^1H\}$ CP-MAS NMR spectrum of **Pt-OM@TiO_2-m-500** is shown on Fig. S6, revealing the resonance signals which are in agreement with previously reported works [47,52,57]. The ratio of C to Pt was found from elemental analysis to be 13:1, which is higher than the calculated one (9:1) for η^1-coordinated species [-O-Pt(COD)Me], suggesting that some pentane solvent was present in the solid.

Hydrogenation of material **Pt-OM@TiO_2-m-500** to generate Pt nanoparticles led to a rapid change of color to dark gray. Methane, ethane and propane were detected by GC as the outlet gases after hydrogenation. In addition, DRIFT spectra showed disappearance of C-H stretching of alkenyl and alkyl groups (Fig. S5c), indicating that cyclooctadiene (COD) and CH_3 were eliminated as hydrogenated volatile byproducts. Meanwhile, the recovery of surface hydroxyls was observed by IR, in line with the expected cleavage of Pt-O bond and formation of Pt nanoparticles (Scheme 1). Therefore, $Pt(COD)Me_2$ can be considered as suitable thermolytic molecular precursor, easily leaving its organic moiety under heat treatment, for preparation of narrowly distributed Pt nanoparticles whose density is mainly determined at the grafting process by the density of hydroxyl groups [76].

TEM analysis of reduced samples prepared by the three different methods were carried out. TEM analysis revealed Pt NPs obtained by grafting technique of around 1 nm with a notably narrower size distribution compared to samples prepared by deposition-precipitation and incipient wetness impregnation methods (Fig. 1 and Table 1). While the deposition-precipitation resulted in similar amount, distribution and size of Pt to the organometallic route, the incipient wetness impregnation showed poor dispersion and formation of large clusters on the surface of titania (Fig. 1).

Crystalline structure and optical properties of Pt-containing catalysts were analysed by XRD and DRS, respectively (Figs. S7, S8). The comparison of the results obtained from XRD, DRS and nitrogen physisorption analysis and collected in Table 1 did not show substantial difference.

Table 1 reports the estimated dispersion, calculated following Borodziński et al. [75] (see SI for more information), and shows the best dispersion with the organometallic route as reported also in literature [47,77]. The reasons of this improved Pt dispersion is believed to be connected to the well-defined surface chemistry between reacting metal precursor and support, avoiding the formation of unreactive species coming from dissolution/precipitation steps when metal salts and metal oxide support are reacting in water [76]. Indeed, grafting the organometallic precursor on controlled surface titanol sites produced mostly

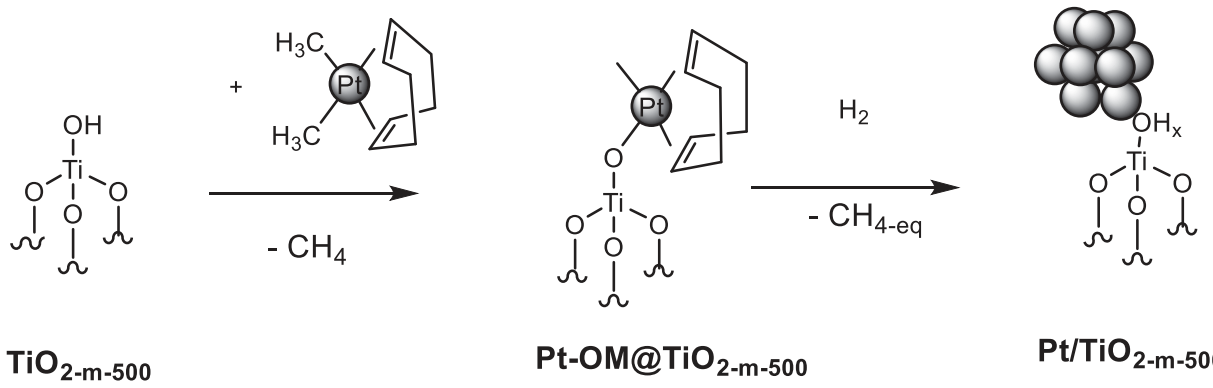

Scheme 1. Overview of the main synthetic route to catalytically performing titania supported highly-dispersed platinum nanoparticles (**Pt/TiO_2-m-500**): Starting dehydroxylated ($T_{dehydrox}$= 500 °C) microemulsion titania (**TiO_2-m-500**, strongly chemisorbed water omitted for simplicity); grafting of the organometallic precursor $PtMe_2$(COD) to yield as major surface species the monoatomic grafted Platinum(II) complex **Pt-OM@TiO_2-m-500**; reduction under dihydrogen.

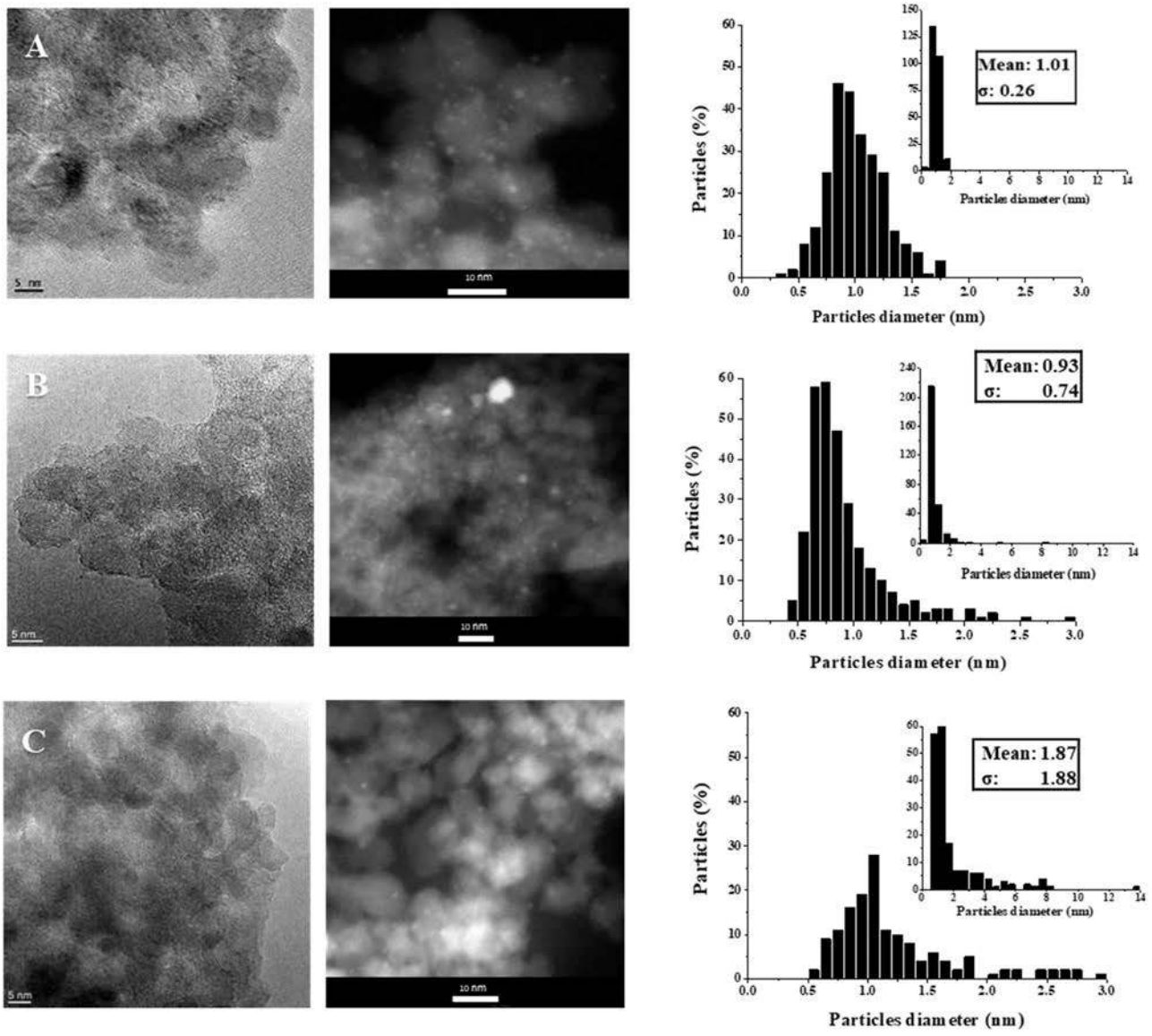

Fig. 1. TEM images and particle size distribution: A) **Pt/ TiO_2-m_SOMC**, B) **Pt/TiO_2-m_DP**, C) **Pt/TiO_2-m_IWI**.

uniform isolated Pt species, avoiding their agglomeration during preparation and also reducing their tendency to sinter when being already in the form of Pt nanoparticles anchored on the TiO_2 support.

In general, the SOMC technique was demonstrated to be able to provide Pt supported catalysts with small active phase, narrow metal size distribution and higher dispersion than samples obtained by standard techniques.

3.3. Photocatalytic test

According to previous investigations [78–82], anaerobic photoreforming of glycerol mainly results in hydrogen production and in the formation of glyceraldehyde, dihydroxyacetone, formaldehyde, glycolaldehyde, hydroxyacetone and acetaldehyde as the principal species in liquid phase.

Fig. 2 shows hydrogen and liquid phase molecules production rates for pristine **TiO_2-m** and supported Pt NPs by different methods. Pt addition provided a significant enhancement of the rate of hydrogen production compared to the bare support. This enhancement is associated to the migration of photo-excited electrons from the conduction band of TiO_2 onto the supported metal nanoparticles, participating in proton reduction, and the ensuing rate decrease of electron-hole recombination phenomena [18,34,81,83].

The use of Pt co-catalyst permitted formation of detectable amount of liquid phase products such as glyceraldehyde and glycolaldehyde, which were the main compounds observed in these conditions. It is worth mentioning that **Pt/TiO_2-m_SOMC** exhibited slightly different rates ratio of liquid phase products. Fig. 2 shows that the difference in the rates of glycolaldehyde and glyceraldehyde formation for **Pt/TiO_2-m_SOMC** sample is not as evident as for **Pt/TiO_2-m_IWI** and **Pt/TiO_2-m_DP**. Changes in acidity have been reported to be among the causes, because they lead to a different cooperative effect of Pt and support. At the same time, literature reports that solid oxides outgassed in different conditions do not change the acidity properties, so this parameter should not be the leading reason for our observed data [84]. As discussed below, the better dispersion might be the main reason (see Figs. 3 and 4).

Formic acid in liquid phase and CO_2, CO and CH_4 in gas phase were also detected in trace amount. No activity was observed when the reactions were performed in dark or when only visible light (> 420 nm) was used. Although the process of light-driven conversion of glycerol is

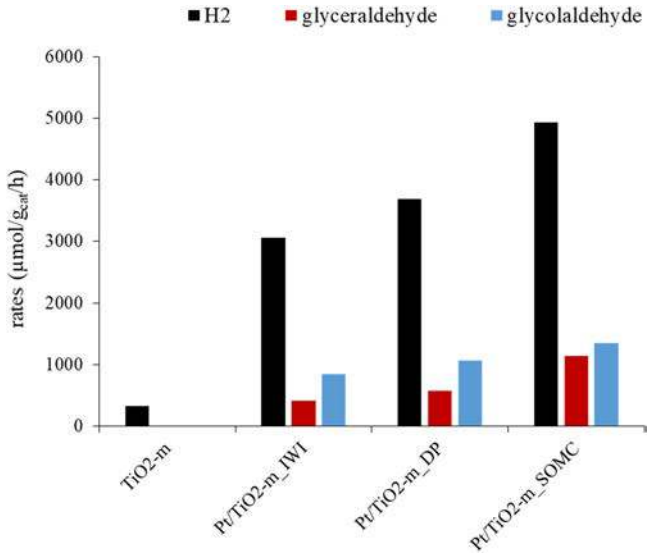

Fig. 2. Rate of hydrogen production and liquid phase products for Pt NPs supported on **TiO_2-m** by incipient wetness impregnation (IWI), deposition-precipitation (DP) methods and Surface Organometallic Chemistry approach (SOMC). 1 M aqueous solution of glycerol, 30 °C; 6 h, 0.5 g/L catalyst loading.

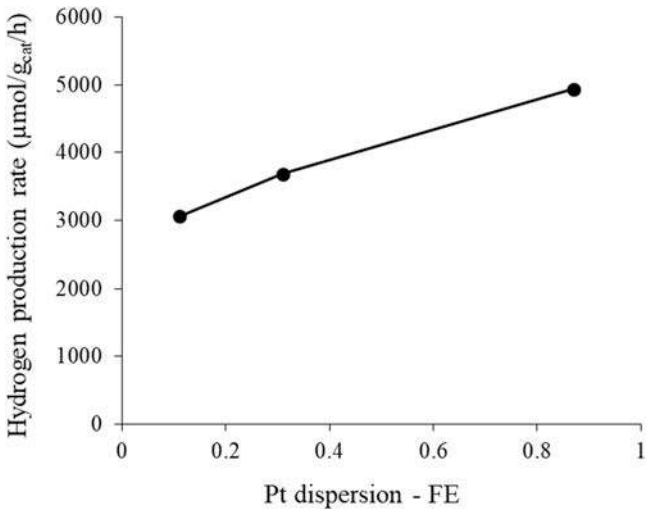

Fig. 3. Dependence of hydrogen production vs. Pt dispersion (FE).

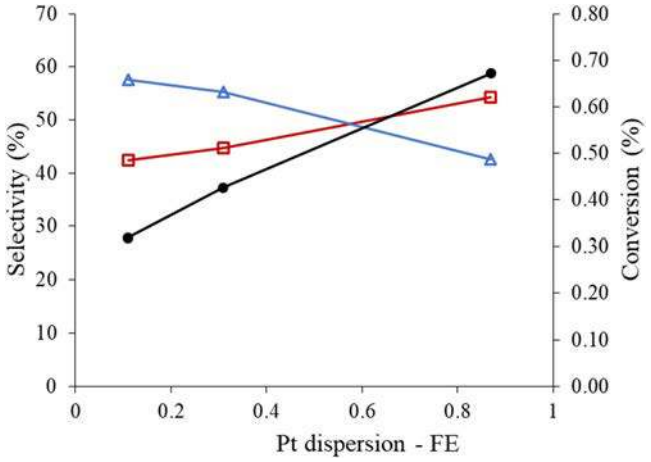

Fig. 4. Dependence of conversion and selectivity vs. Pt dispersion (FE).Legend: glycerol (●), glyceraldehyde (□), glycolaldehyde (△).

complex, meaning the production of multiple intermediates and different rates of their formation, a common feature for all the mechanisms is the formation of glyceraldehyde and glycolaldehyde among the primary products [78,79,85–88], which is compatible with observed data (Scheme 2).

The formation of glyceraldehyde as one of the primary products is believed to take place via indirect mechanism described by Sanwald and co-workers using Rh NPs supported on commercial titania P25 [78]. In principle, the photo-generated holes are trapped by lattice oxygen sites in TiO_2, abstracting the H-atom from C–H bond with subsequent formation of carbonyl group. One molecule of hydrogen is produced concurrently at a cathodic site. Further oxidation of glyceraldehyde can yield glycolaldehyde and formic acid. On the other hand, glycolaldehyde can be formed also via direct C–C cleavage of glycerol as was reported by Minero [87], starting from a hole transfer to a chemisorbed glycerol on coordinatively unsaturated Ti(IV)-OH site to generate an alkoxide radical followed by β-C–C-scission. Thus, hydrogen and glyceraldehyde formation are favored in the presence of both Pt and TiO_2, while glycolaldehyde production can occur on sole titania. For this reason a higher rate of hydrogen production and glyceraldehyde formation are observed at higher Pt dispersions. Further oxidation of glyceraldehyde to glycolaldehyde probably provides a concurrent increase in the rate formation of the latter.

As seen in Fig. 2, higher H_2 production rates were obtained with the

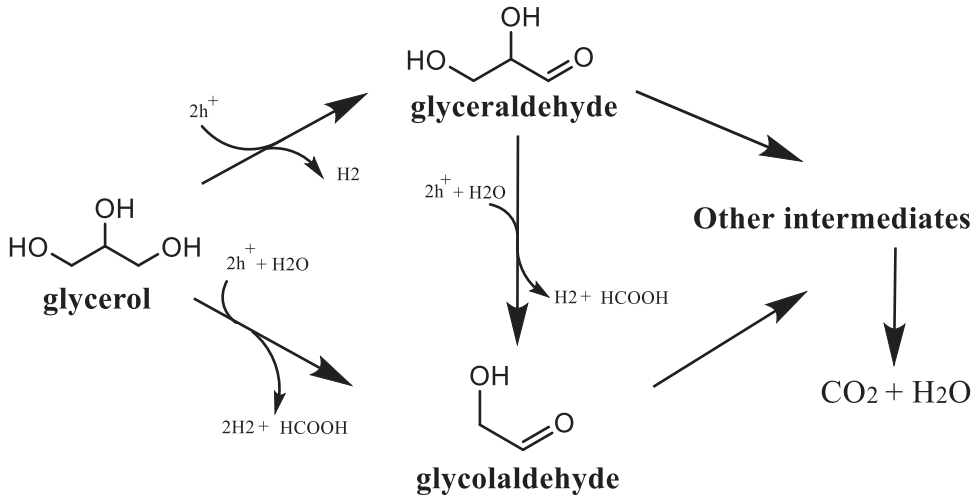

Scheme 2. Suggested mechanism of glycerol oxidative photo-dehydrogenation. Adapted from [78,79,84–87].

sample prepared by SOMC. In order to verify the absence of leaching of Pt, ICP analysis was carried out on the reaction solution after centrifugation to remove the solid catalyst and the analysis confirmed the absence of Pt in the reaction mixture.

A correlation between hydrogen productivity and Pt dispersion for tested materials is shown in Fig. 3, suggesting that improved hydrogen production rate could be correlated to better homogeneously dispersed Pt NPs on titania surface. Analysis of selectivity of liquid phase products showed a decrease of glycolaldehyde and an increase of glyceraldehyde selectivity together with glycerol conversion as the Pt dispersion improves (Fig. 4). Comparing the data from XRD, N_2 physisorption, TEM and DRS one can suggest that conversion of glycerol and glyceraldehyde selectivity increase by the type of preparation method from IWI < DP < SOMC as the dispersion of Pt NPs over **TiO_2-m** improves, confirming the importance of deposition method on the metal dispersion on the surface of titania. The stability of the catalyst was confirmed by performing consecutive tests using **Pt/TiO_2-m_SOMC** (Fig. S9). The catalyst proved to be active in the reuse tests showing hydrogen productivities comparable to the first one.

Comparison of literature reports on hydrogen production using oxygenates by means of heterogeneous photocatalysis is complicated task because of the differences in light sources, geometry of photoreactors and reaction conditions used by different research groups. Recently, protocols and standardization to report the results in the field of heterogeneous photocatalysis have been proposed [89,90]. In an attempt to compare obtained results with the state of the art, different literature reports on hydrogen production from glycerol using platinum supported titania are summarized in Table 2. Comparing similar light source, glycerol and catalyst loading, the material prepared in this work outperformed the systems reported up to date [32,33,91]. On one side, this could be explained by a higher loading of Pt nanoparticles, which play role as active sites capable of proton reduction. Nevertheless, the results of H_2 production obtained for different Pt loading did not increase proportionally to the metal content [35,88], and in fact, in the range of 1–2 wt% of Pt the rate of H_2 production was found to be comparable [11]. With the further increase of amount of metal co-catalyst the hydrogen production may decrease due to following reasons: decreased light absorption by titania surface (shading effect), decreased surface area of the metal co-catalyst due to the particles agglomeration, reduced metal co-catalyst dispersion on the surface of TiO_2 [9]. Thereby, improved photocatalytic activity in this work could be mainly explained by a high specific surface area of titania prepared by microemulsion, giving access to the increased densities of active sites and the high dispersion of Pt given by the SOMC technique. In fact, if the amount of glycerol and Pt added is taken into account in the hydrogen rate equation (Rate H_2 in mmol/g_{gly}/g_{Pt}/h), the catalyst developed in this work highly outperforms other Pt/TiO_2 tested in similar conditions, evidencing that the high activity is not solely due to the Pt loading.

4. Conclusions

Organometallic complex Pt(COD)Me_2 was grafted on the surface of

Table 2
Comparison of photocatalytic hydrogen production obtained in this work with results reported in the literature at similar conditions (Pt/TiO_2, Xe lamp).

Type of titania	S_{TiO2}, g/m^2	Pt NPs[a]	wt% Pt	d_{Pt}, nm	Catalyst loading, g/L	Glycerol loading, %vol.	Rate H_2, mmol/g_{cat}/h	Rate H_2, mmol/g_{gly}/g_{Pt}/h	Source	Ref
P25 (Evonik Degussa)	49	IWI, H_2	1	1.8	0.6	3.2	3.30	55	300 W Xe	[33,92]
		PD		2.2			2.04	34		
		In situ PD		2.0			4.28	71		
TiO_2 (hydrothermal)	71	*In situ* PD	0.2	1–3	0.6	7	1.3	92	150 W Xe	[90]
P25 (Evonik Degussa)	41	IWI, H_2	0.5	1.2	1.3	8.1	2.7	18	300 W Xe	[32,87]
TiO_2-m	164	DP, H_2	1.5	0.9	0.5	7.2	3.68	125	300 W Xe	This work
		IWI, H_2		1.9			3.06	104		
		SOMC, H_2		1.0			4.93	167		

[a] Method of Pt NPs preparation: IWI, H_2 – impregnation of platinum salt with subsequent reduction in hydrogen; PD and in situ PD – photodeposition and in situ reduction prepared in different conditions; DP, H_2 – deposition-precipitation with subsequent reduction in hydrogen; SOMC, H_2 – grafting of SOMC complex with subsequent reduction in hydrogen.

TiO_2-m prepared from reverse microemulsion system. The prepared material was then reduced in hydrogen forming well-defined Pt nanoparticles with a small 1 nm size, and a narrow size distribution. The presence Pt NPs on the surface of titania efficiently reduced electron-hole recombination and enhanced the hydrogen evolution as well as liquid phase products formation, namely glyceraldehyde and glycolaldehyde. The prepared sample outperformed in the reaction of glycerol oxidative photo-dehydrogenation the samples with Pt deposited by incipient wetness impregnation and deposition-precipitation owing to a better dispersion of Pt nanoparticles. Besides, it has been observed that the dispersion can affect the selectivity of liquid phase products together with hydrogen production rate. With increase of Pt dispersion H_2 productivity raised, selectivity of glycolaldehyde decreased, while glyceraldehyde selectivity increased. Comparison of the obtained results on hydrogen productivity with the state of the art revealed that high surface area of support obtained by microemulsion synthesis and highly dispersed ultrafine Pt NPs given by SOMC method improved the photocatalytic performance, providing hydrogen productivities higher than previously reported works.

CRediT authorship contribution statement

Valeriia Maslova: Investigation, Data curation, Writing Original draft preparation. **Elsje Alessandra Quadrelli**: Supervision, Conceptualization, Methodology. **Pooja Gaval**: Software, investigation, Resources. ˙ **Andrea Fasolini**: software, data curation, Resources. **Stefania Albonetti**: Supervision, Writing- Reviewing and Editing, Funding acquisition. **Francesco Basile**: Conceptualization, Methodology, validation.

Declaration of Competing Interest

The authors declare that they have no known competing financial interests or personal relationships that could have appeared to influence the work reported in this paper.

Acknowledgment

This work was co-funded through an Education, Audiovisual and Culture Executive Agency (EACEA) Erasmus Mundus grant (SINCHEM Programme). SINCHEM is a Joint Doctorate programme selected under the Erasmus Mundus Action 1 Programme (FPA 2013-0037). We thank Francesca Ospitali, Department of Industrial Chemistry "Toso Montanari", Università di Bologna, and Laurent Veyre, C2P2, Université de Lyon 1, for assistance with TEM analysis. We also thank Alessandra Petroli, Department of Industrial Chemistry "Toso Montanari", Università di Bologna, for assistance with NMR analysis. As well as Ruben Vera, CDHL, Université de Lyon 1, for assistance with XRD analysis.

Appendix A. Supporting information

Supplementary data associated with this article can be found in the online version at doi:10.1016/j.jece.2021.105070.

References

[1] P. Lanzafame, S. Abate, C. Ampelli, C. Genovese, R. Passalacqua, G. Centi, S. Perathoner, Beyond solar fuels: renewable energy-driven chemistry, ChemSusChem 10 (2017) 4409–4419, https://doi.org/10.1002/cssc.201701507.
[2] G. Bagnato, A. Iulianelli, A. Sanna, A. Basile, Glycerol production and transformation: a critical review with particular emphasis on glycerol reforming reaction for producing hydrogen in conventional and membrane reactors, Membranes 7 (2017) 1–31, https://doi.org/10.3390/membranes7020017.
[3] G. Dodekatos, S. Schünemann, H. Tüysüz, Recent advances in thermo-, photo-, and electrocatalytic glycerol oxidation, ACS Catal. 8 (2018) 6301–6333, https://doi.org/10.1021/acscatal.8b01317.
[4] B. Victor, T. Ab, R. Bin, T. Abdullah, M. Ali, S. Indati, S. Fatihah, Recent advances in renewable hydrogen production by thermo-catalytic conversion of biomass-derived glycerol: overview of prospects and challenges, Int. J. Hydrog. Energy 45 (2019) 18160–18185, https://doi.org/10.1016/j.ijhydene.2019.08.002.
[5] Q. (Sophia) He, J. McNutt, J. Yang, Utilization of the residual glycerol from biodiesel production for renewable energy generation, Renew. Sustain. Energy Rev. 71 (2017) 63–76, https://doi.org/10.1016/j.rser.2016.12.110.
[6] F. Basile, S. Albonetti, F. Cavani, E. Lombardi, R. Mafessanti, Biosyngas and derived products from gasification and aqueous phase reforming. Chem. Fuels Bio-Based Build. Blocks, 2016, pp. 79–110.
[7] Y.C. Lin, Catalytic valorization of glycerol to hydrogen and syngas, Int. J. Hydrog. Energy 38 (2013) 2678–2700, https://doi.org/10.1016/j.ijhydene.2012.12.079.
[8] A.V. Puga, Photocatalytic production of hydrogen from biomass-derived feedstocks, Coord. Chem. Rev. (2016) 1–66, https://doi.org/10.1016/j.ccr.2015.12.009.
[9] K.C. Christoforidis, P. Fornasiero, Photocatalytic hydrogen production: a rift into the future energy supply, ChemCatChem 9 (2017) 1523–1544, https://doi.org/10.1002/cctc.201601659.
[10] X. Fu, X. Wang, D.Y.C. Leung, Q. Gu, S. Chen, H. Huang, Photocatalytic reforming of C3-polyols for H2 production Part (I). Role of their OH groups, Appl. Catal. B Environ. 106 (2011) 681–688, https://doi.org/10.1016/j.apcatb.2011.05.045.
[11] V.M. Daskalaki, D.I. Kondarides, Efficient production of hydrogen by photo-induced reforming of glycerol at ambient conditions, Catal. Today 144 (2009) 75–80, https://doi.org/10.1016/j.cattod.2008.11.009.
[12] V. Augugliaro, H.A.H. El Nazer, V. Loddo, A. Mele, G. Palmisano, L. Palmisano, S. Yurdakal, Partial photocatalytic oxidation of glycerol in TiO2 water suspensions, Catal. Today 151 (2010) 21–28, https://doi.org/10.1016/j.cattod.2010.01.022.
[13] M. Stelmachowski, M. Marchwicka, E. Grabowska, M. Diak, The photocatalytic conversion of (biodiesel derived) glycerol to hydrogen - A short review and preliminary experimental results part 2: photocatalytic conversion of glycerol to hydrogen in batch and semi-batch laboratory reactors, J. Adv. Oxid. Technol. 17 (2014) 179–186.
[14] T.W.P. Seadira, G. Sadanandam, T. Ntho, C.M. Masuku, M.S. Scurrell, Preparation and characterization of metals supported on nanostructured TiO2 hollow spheres for production of hydrogen via photocatalytic reforming of glycerol, Appl. Catal. B Environ. 222 (2018) 133–145, https://doi.org/10.1016/j.apcatb.2017.09.072.
[15] H.X. Sang, X.T. Wang, C.C. Fan, F. Wang, Enhanced photocatalytic H2 production from glycerol solution over ZnO/ZnS core/shell nanorods prepared by a low temperature route, Int. J. Hydrog. Energy 37 (2011) 1348–1355, https://doi.org/10.1016/j.ijhydene.2011.09.129.
[16] V. Vaiano, G. Iervolino, Photocatalytic hydrogen production from glycerol aqueous solution using Cu-Doped ZnO under visible light irradiation, Appl. Sci. 9 (2019) 2741, https://doi.org/10.3390/app9132741.
[17] G. Carraro, C. MacCato, A. Gasparotto, T. Montini, S. Turner, O.I. Lebedev, V. Gombac, G. Adami, G. Van Tendeloo, D. Barreca, P. Fornasiero, Enhanced hydrogen production by photoreforming of renewable oxygenates through nanostructured Fe2O3 polymorphs, Adv. Funct. Mater. 24 (2014) 372–378, https://doi.org/10.1002/adfm.201302043.
[18] A.G. Dosado, W.T. Chen, A. Chan, D. Sun-Waterhouse, G.I.N. Waterhouse, Novel Au/TiO2 photocatalysts for hydrogen production in alcohol–water mixtures based on hydrogen titanate nanotube precursors, J. Catal. 330 (2015) 238–254, https://doi.org/10.1016/j.jcat.2015.07.014.
[19] R.P. Panmand, Y.A. Sethi, S.R. Kadam, M.S. Tamboli, L.K. Nikam, J.D. Ambekar, C.-J. Park, B.B. Kale, Self-assembled hierarchical nanostructures of Bi2WO6 for hydrogen production and dye degradation under solar light, CrystEngComm 17 (2015) 107–115, https://doi.org/10.1039/C4CE01968G.
[20] X. Zong, G. Wu, H. Yan, G. Ma, J. Shi, F. Wen, L. Wang, C. Li, Photocatalytic H2 evolution on MoS2/CdS catalysts under visible light irradiation, J. Phys. Chem. C 114 (2010) 1963–1968.
[21] M. De Oliveira, L. Almeida, Visible light-induced hydrogen production from glycerol aqueous solution on hybrid Pt–CdS–TiO2 photocatalysts, J. Photochem. Photobiol. A Chem. 226 (2011) 36–41, https://doi.org/10.1016/j.jphotochem.2011.10.012.
[22] X.T. Wang, R. Lv, K. Wang, Synthesis of ZnO@ZnS-Bi2S3 core-shell nanorod grown on reduced graphene oxide sheets and its enhanced photocatalytic performance, J. Mater. Chem. A 2 (2014) 8304–8313, https://doi.org/Doi 10.1039/C4ta00696h.
[23] A. Petala, E. Ioannidou, A. Georgaka, K. Bourikas, D.I. Kondarides, Hysteresis phenomena and rate fluctuations under conditions of glycerol photo-reforming reaction over CuOx/TiO2 catalysts, Appl. Catal. B Environ. 178 (2015) 201–209, https://doi.org/10.1016/j.apcatb.2014.09.021.
[24] V. Gombac, L. Sordelli, T. Montini, J.J. Delgado, A. Adamski, G. Adami, M. Cargnello, S. Bernal, P. Fornasiero, CuOx−TiO2 photocatalysts for H2 production from ethanol and glycerol solutions, J. Phys. Chem. A 114 (2010) 3916–3925, https://doi.org/10.1021/jp907242q.
[25] Y. Li, B. Wang, S. Liu, X. Duan, Z. Hu, Synthesis and characterization of Cu2O/TiO2 photocatalysts for H2 evolution from aqueous solution with different scavengers,, Appl. Surf. Sci. 324 (2015) 736–744, https://doi.org/10.1016/j.apsusc.2014.11.027.
[26] D. Praveen Kumar, N. Lakshmana Reddy, M. Mamatha Kumari, B. Srinivas, V. Durga Kumari, B. Sreedhar, V. Roddatis, O. Bondarchuk, M. Karthik, B. Neppolian, M.V. Shankar, Cu2O-sensitized TiO2 nanorods with nanocavities for highly efficient photocatalytic hydrogen production under solar irradiation, Sol. Energy Mater. Sol. Cells 136 (2015) 157–166, https://doi.org/10.1016/j.solmat.2015.01.009.
[27] J. Yu, Y. Hai, M. Jaroniec, Photocatalytic hydrogen production over CuO-modified titania, J. Colloid Interface Sci. 357 (2011) 223–228, https://doi.org/10.1016/j.jcis.2011.01.101.

[28] J. Hidalgo-Carrillo, J. Martin-Gomez, J. Morales, J.C. Espejo, F.J. Urbano, A. Marinas, Hydrogen photo-production from glycerol using nickel-doped TiO2 catalysts: effect of catalyst pre-treatment, Energies 12 (2019) 3351.

[29] S. Ichiro Fujita, H. Kawamori, D. Honda, H. Yoshida, M. Arai, Photocatalytic hydrogen production from aqueous glycerol solution using NiO/TiO2 catalysts: effects of preparation and reaction conditions, Appl. Catal. B Environ. 181 (2016) 818–824, https://doi.org/10.1016/j.apcatb.2015.08.048.

[30] M. Yasuda, T. Matsumoto, T. Yamashita, Sacrificial hydrogen production over TiO2-based photocatalysts: polyols, carboxylic acids, and saccharides, Renew. Sustain. Energy Rev. 81 (2018) 1627–1635.

[31] Z.H.N. Al-Azri, W. Chen, A. Chan, V. Jovic, T. Ina, H. Idriss, G.I.N. Waterhouse, The roles of metal co-catalysts and reaction media in photocatalytic hydrogen production: performance evaluation of M/TiO2 photocatalysts (M = Pd, Pt, Au) in different alcohol – water mixtures, J. Catal. 329 (2015) 355–367.

[32] D.I. Kondarides, V.M. Daskalaki, A. Patsoura, X.E. Verykios, Hydrogen production by photo-induced reforming of biomass components and derivatives at ambient conditions, Catal. Lett. 122 (2008) 26–32, https://doi.org/10.1007/s10562-007-9330-3.

[33] X. Jiang, X. Fu, L. Zhang, S. Meng, S. Chen, Photocatalytic reforming of glycerol for H2 evolution on Pt/TiO2: fundamental understanding the effect of co-catalyst Pt and the Pt deposition route, J. Mater. Chem. A 3 (2015) 2271–2282, https://doi.org/10.1039/C4TA06052K.

[34] W. Chen, A. Chan, Z.H.N. Al-Azri, A.G. Dosado, M.A. Nadeem, D. Sun-Waterhouse, H. Idriss, G.I.N. Waterhouse, Effect of TiO2 polymorph and alcohol sacrificial agent on the activity of Au/TiO2 photocatalysts for H2 production in alcohol – water mixtures, J. Catal. 329 (2015) 499–513, https://doi.org/10.1016/j.jcat.2015.06.014.

[35] F.J. López-Tenllado, J. Hidalgo-Carrillo, V. Montes, A. Marinas, F.J. Urbano, J. M. Marinas, L. Ilieva, T. Tabakova, F. Reid, A comparative study of hydrogen photocatalytic production from glycerol and propan-2-ol on M/TiO2 systems (M=Au, Pt, Pd), Catal. Today 280 (2017) 58–64, https://doi.org/10.1016/j.cattod.2016.05.009.

[36] H. Bahruji, M. Bowker, P.R. Davies, L.S. Al-Mazroai, A. Dickinson, J. Greaves, D. James, L. Millard, F. Pedrono, Sustainable H2 gas production by photocatalysis, J. Photochem. Photobiol. A Chem. 216 (2010) 115–118, https://doi.org/10.1016/j.jphotochem.2010.06.022.

[37] Z.H.N. Al-Azri, W.T. Chen, A. Chan, V. Jovic, T. Ina, H. Idriss, G.I.N. Waterhouse, The roles of metal co-catalysts and reaction media in photocatalytic hydrogen production: performance evaluation of M/TiO2 photocatalysts (M = Pd, Pt, Au) in different alcohol–water mixtures, J. Catal. 329 (2015) 355–367, https://doi.org/10.1016/j.jcat.2015.06.005.

[38] G.I.N. Waterhouse, W. Chen, A. Chan, D. Sun-waterhouse, J. Llorca, H. Idriss, Performance comparison of Ni/TiO2 and Au/TiO2 photocatalysts for H2 production in different alcohol-water mixtures, J. Catal. 367 (2018) 27–42, https://doi.org/.1037//0033-2909.I26.1.78.

[39] M. Wang, M. Liu, J. Lu, F. Wang, Photo splitting of bio-polyols and sugars to methanol and syngas, Nat. Commun. 11 (2020) 1–9, https://doi.org/10.1038/s41467-020-14915-8.

[40] K. Shimura, H. Yoshida, Heterogeneous photocatalytic hydrogen production from water and biomass derivatives, Energy Environ. Sci. 4 (2011) 2467–2481, https://doi.org/10.1039/c1ee01120k.

[41] E.A. Quadrelli, J.M. Basset, On silsesquioxanes' accuracy as molecular models for silica-grafted complexes in heterogeneous catalysis, Coord. Chem. Rev. 254 (2010) 707–728, https://doi.org/10.1016/j.ccr.2009.09.031.

[42] C. Copéret, M. Chabanas, R. Petroff Saint-Arroman, J.M. Basset, Surface organometallic chemistry: Homogeneous and heterogeneous catalysis: bridging the gap through surface organometallic chemistry, Angew. Chem. Int. Ed. 42 (2003) 156–181, https://doi.org/10.1002/anie.200390072.

[43] C. Copéret, A. Comas-Vives, M.P. Conley, D.P. Estes, A. Fedorov, V. Mougel, H. Nagae, F. Núnez-Zarur, P.A. Zhizhko, Surface organometallic and coordination chemistry toward single-site heterogeneous catalysts: strategies, methods, structures, and activities, Chem. Rev. 116 (2016) 323–421, https://doi.org/10.1021/acs.chemrev.5b00373.

[44] J.-M. Basset, A. Baudouin, F. Bayard, J.-P. Candy, C. Copret, D.A. Mallmann, G. Godard, E. Kuntz, F. Lefebvre, C. Lucas, S. Norsic, K. Pelzer, A. Quadrelli, C. Santini, D. Soulivong, F. Stoffelbach, M. Taoufik, C. Thieuleux, J. Thivolle-Cazat, L. Veyre, Preparation of single site catalysts on oxides and metals prepared via surface organometallic chemistry. Modern Surface Organometallic Chemistry, 2009, pp. 23–73.

[45] M.K. Samantaray, E. Pump, A. Bendjeriou-Sedjerari, V. D'Elia, J.D.A. Pelletier, M. Guidotti, R. Psaro, J.M. Basset, Surface organometallic chemistry in heterogeneous catalysis, Chem. Soc. Rev. 47 (2018) 8403–8437, https://doi.org/10.1039/c8cs00356d.

[46] Y. Iwasawa, H. Sato, Preparations of TiO2-attached Rh catalysts and their catalysis, Chem. Lett. 14 (1985) 507–510.

[47] P. Laurent, L. Veyre, C. Thieuleux, S. Donet, C. Copéret, From well-defined Pt(II) surface species to the controlled growth of silica supported Pt nanoparticles, Dalton Trans. 42 (2013) 238–248, https://doi.org/10.1039/c2dt31639k.

[48] K. Philippot, B. Chaudret, Organometallic approach to the synthesis and surface reactivity of noble metal nanoparticles, C. R. Chim. 6 (2003) 1019–1034, https://doi.org/10.1016/j.crci.2003.07.010.

[49] T. Andana, M. Piumetti, S. Bensaid, L. Veyre, C. Thieuleux, N. Russo, D. Fino, A. E. Quadrelli, R. Pirone, Ceria-supported small Pt and Pt3Sn nanoparticles for NOx -assisted soot oxidation, Appl. Catal. B Environ. 209 (2017) 295–310, https://doi.org/10.1016/j.apcatb.2017.03.010.

[50] T. Andana, M. Piumetti, S. Bensaid, L. Veyre, C. Thieuleux, N. Russo, D. Fino, E. Alessandra, R. Pirone, CuO nanoparticles supported by ceria for NOx-assisted soot oxidation: insight into catalytic activity and sintering, Appl. Catal. B Environ. 216 (2017) 41–58, https://doi.org/10.1016/j.apcatb.2017.05.061.

[51] T. Andana, M. Piumetti, S. Bensaid, L. Veyre, C. Thieuleux, N. Russo, D. Fino, E. Alessandra, Nanostructured equimolar ceria-praseodymia for NOx -assisted soot oxidation: Insight into Pr dominance over Pt nanoparticles and metal – support interaction, Appl. Catal. B Environ. 226 (2018) 147–161, https://doi.org/10.1016/j.apcatb.2017.12.048.

[52] M.L.M. Bonati, T.M. Douglas, S. Gaemers, N. Guo, Synthesis, characterization, and catalytic properties of novel single-site and nanosized platinum catalysts, Organometallics 31 (2012) 5243–5251, https://doi.org/10.1021/om200778r.

[53] M. Boualleg, J.-M. Basset, J.-P. Candy, V. Caps, J.-C. Jumas, S. Norsic, E. A. Quadrelli, L. Veyre, C. Thieuleux, Single-phase heterogeneous Pt3Sn catalyst synthesized by room-temperature self-assembly, ChemCatChem 4 (2012) 1729–1732, https://doi.org/10.1002/cctc.201200276.

[54] K. Pelzer, M. Hävecker, M. Boualleg, J.-P. Candy, J.M. Basset, Stabilization of 200-atom platinum nanoparticles by organosilane Fragments, Angew. Chem. Int. Ed. 50 (2011) 5170–5173, https://doi.org/10.1002/anie.201008209.

[55] T. Galeandro-Diamant, I. Suleimanov, L. Veyre, M. Bousquie, V. Meille, C. Thieuleux, Alkene hydrosilylation with supported and unsupported Ni nanoparticles: strong influence of the Ni environment on activity and selectivity, Catal. Sci. Technol. 9 (2019) 1555–1558.

[56] H.S. Ahn, J. Yano, T.D. Tilley, Water oxidation by cobalt centers on various oxide surfaces: the effects of oxide surface acidity and oxygen atom affinity on catalysis, ACS Catal. 5 (2015) 2573–2576, https://doi.org/10.1021/cs502120f.

[57] G. Jeantelot, M. Qureshi, M. Harb, S. Ould-Chikh, D.H. Anjum, E. Abou-Hamad, A. Aguilar-Tapia, J.L. Hazemann, K. Takanabe, J.M. Basset, TiO2-supported Pt single atoms by surface organometallic chemistry for photocatalytic hydrogen evolution, Phys. Chem. Chem. Phys. 21 (2019) 24429–24440, https://doi.org/10.1039/c9cp04470a.

[58] M. Qureshi, A.T. Garcia-Esparza, G. Jeantelot, S. Ould-Chikh, A. Aguilar-Tapia, J. L. Hazemann, J.M. Basset, D. Loffreda, T. Le Bahers, K. Takanabe, Catalytic consequences of ultrafine Pt clusters supported on SrTiO3 for photocatalytic overall water splitting, J. Catal. 376 (2019) 180–190, https://doi.org/10.1016/j.jcat.2019.06.045.

[59] M. Andersson, A. Kiselev, L. Österlund, A.E.C. Palmqvist, Microemulsion-mediated room-temperature synthesis of high-surface-area rutile and its photocatalytic performance, J. Phys. Chem. C 111 (2007) 6789–6797, https://doi.org/10.1021/jp070284a.

[60] H. Kisch, Korrespondenz on the problem of comparing rates or apparent quantum yields in heterogeneous photocatalysis, Angew. Chem. 122 (2010) 9782–9783, https://doi.org/10.1002/ange.201002653.

[61] D. Das, A. Shivhare, S. Saha, A.K. Ganguli, Room temperature synthesis of mesoporous TiO2 nanostructures with high photocatalytic efficiency, Mater. Res. Bull. 47 (2012) 3780–3785.

[62] J. Carbajo, A. Bahamonde, M. Faraldos, Photocatalyst performance in wastewater treatment applications: towards the role of TiO2 properties, Mol. Catal. 434 (2017) 167–174.

[63] F. Basile, R. Mafessanti, A. Fasolini, G. Fornasari, E. Lombardi, A. Vaccari, Effect of synthetic method on CeZr support and catalytic activity of related Rh catalyst in the oxidative reforming reaction, J. Eur. Ceram. Soc. 39 (2019) 41–52, https://doi.org/10.1016/j.jeurceramsoc.2018.01.047.

[64] K.A.R. Joseph, B. Viswanathan, Effect of surface area, pore volume and particle size of P25 titania on the phase transformation of anatase to rutile, Indian J. Chem. - Sect. A Inorg. Phys. Theor. Anal. Chem. 48 (2009) 1378–1382.

[65] D. Nguyen Thanh, O. Kikhtyanin, R. Ramos, M. Kothari, P. Ulbrich, T. Munshi, D. Kubička, Nanosized TiO2 – A promising catalyst for the aldol condensation of furfural with acetone in biomass upgrading, Catal. Today 277 (2016) 97–107, https://doi.org/10.1016/j.cattod.2015.11.027.

[66] C. Arrouvel, M. Digne, M. Breysse, H. Toulhoat, P. Raybaud, Effects of morphology on surface hydroxyl concentration: a DFT comparison of anatase-TiO2 and γ-alumina catalytic supports, J. Catal. 222 (2004) 152–166, https://doi.org/10.1016/j.jcat.2003.10.016.

[67] H. Huang, J. Lin, L. Fan, X. Wang, X. Fu, J. Long, Heteroatomic Ni, Sn clusters-grafted anatase TiO2 photocatalysts: structure, electron delocalization, and synergy for solar hydrogen production, J. Phys. Chem. C 119 (2015) 10478–10492, https://doi.org/10.1021/acs.jpcc.5b02256.

[68] K. Tanaka, J.M. White, Characterization of species adsorbed on oxidized and reduced anatase, J. Phys. Chem. 86 (1982) 4708–4714, https://doi.org/10.1021/j100221a014.

[69] K.S. Finnie, D.J. Cassidy, J.R. Bartlett, J.L. Woolfrey, IR spectroscopy of surface water and hydroxyl species on nanocrystalline TiO2 films, Langmuir 17 (2001) 816–820, https://doi.org/10.1021/la0009240.

[70] P. Sampedro, G. Colón, M. Fernández-García, Visible-light driven TiO2 photocatalysts from Ti-oxychloride precursors, J. Photochem. Photobiol. A Chem. 199 (2008) 136–143, https://doi.org/10.1016/j.jphotochem.2008.05.008.

[71] W. Jiang, M. Zhang, J. Wang, Y. Liu, Y. Zhu, Dramatic visible activity in phenol degradation of TCNQ at TiO2 photocatalyst with core-shell structure, Appl. Catal. B Environ. 160–161 (2014) 44–50, https://doi.org/10.1016/j.apcatb.2014.04.050.

[72] F. Chen, W. Zou, W. Qu, J. Zhang, Photocatalytic performance of a visible light TiO2 photocatalyst prepared by a surface chemical modification process, Catal. Commun. 10 (2009) 1510–1513, https://doi.org/10.1016/j.catcom.2009.04.005.

[73] K. Yamakawa, Y. Sato, K. Fukutani, Asymmetric and symmetric absorption peaks observed in infrared spectra of CO_2 adsorbed on TiO2 nanotubes, J. Chem. Phys. 144 (7) (2016), 154703, https://doi.org/10.1063/1.4946790.

[74] Y. Cao, S. Hu, M. Yu, S. Yan, M. Xu, Adsorption and interaction of CO_2 on rutile TiO2 (110) surfaces: a combined UHV-FTIRS and theoretical simulation study, Phys. Chem. Chem. Phys. 17 (2015) 23994–24000, https://doi.org/10.1039/c5cp04013b.
[75] A. Borodziński, M. Bonarowska, Relation between crystallite size and dispersion on supported metal catalysts, Langmuir 13 (1997) 5613–5620, https://doi.org/10.1021/la962103u.
[76] C. Copéret, Single-sites and nanoparticles at tailored interfaces prepared via surface organometallic chemistry from thermolytic molecular precursors, Acc. Chem. Res. 52 (2019) 1697–1708, https://doi.org/10.1021/acs.accounts.9b00138.
[77] L. Rochlitz, K. Searles, J. Alfke, D. Zemlyanov, O.V. Safonova, C. Copéret, Silica-supported, narrowly distributed, subnanometric Pt-Zn particles from single sites with high propane dehydrogenation performance, Chem. Sci. 11 (2020) 1549–1555, https://doi.org/10.1039/c9sc05599a.
[78] K.E. Sanwald, T.F. Berto, W. Eisenreich, O.Y. Gutiérrez, J.A. Lercher, Catalytic routes and oxidation mechanisms in photoreforming of polyols, J. Catal. 344 (2016) 806–816, https://doi.org/10.1016/j.jcat.2016.08.009.
[79] R. Chong, J. Li, X. Zhou, Y. Ma, J. Yang, L. Huang, H. Han, F. Zhang, C. Li, Selective photocatalytic conversion of glycerol to hydroxyacetaldehyde in aqueous solution on facet tuned TiO2-based catalysts, Chem. Commun. 50 (2014) 165–167, https://doi.org/10.1039/c3cc46515b.
[80] P. Panagiotopoulou, E.E. Karamerou, D.I. Kondarides, Kinetics and mechanism of glycerol photo-oxidation and photo-reforming reactions in aqueous TiO2 and Pt/TiO2 suspensions, Catal. Today 209 (2013) 91–98, https://doi.org/10.1016/j.cattod.2012.09.029.
[81] V. Maslova, A. Fasolini, M. Offidani, S. Albonetti, F. Basile, Solar-driven valorization of glycerol towards production of chemicals and hydrogen, 2021, Submitted for publication.
[82] G.R. Bamwenda, S. Tsubota, T. Nakamura, M. Haruta, Photoassisted hydrogen production from a water-ethanol solution: a comparison of activities of Au-TiO2 and Pt-TiO2, J. Photochem. Photobiol. A Chem. 89 (1995) 177–189.
[83] W.T. Chen, A. Chan, Z.H.N. Al-Azri, A.G. Dosado, M.A. Nadeem, D. Sun-Waterhouse, H. Idriss, G.I.N. Waterhouse, Effect of TiO2 polymorph and alcohol sacrificial agent on the activity of Au/TiO2 photocatalysts for H2 production in alcohol-water mixtures, J. Catal. 329 (2015) 499–513, https://doi.org/10.1016/j.jcat.2015.06.014.
[84] G. Martra, Lewis acid and base sites at the surface of microcrystalline TiO2 anatase: relationships between surface morfology and chemical behavior, Appl. Catal. A 200 (2000) 275–285.
[85] T. Montini, M. Monai, A. Beltram, I. Romero-Ocaña, P. Fornasiero, H2 production by photocatalytic reforming of oxygenated compounds using TiO2-based materials, Mater. Sci. Semicond. Process. 42 (2016) 122–130, https://doi.org/10.1016/j.mssp.2015.06.069.
[86] T. Montini, V. Gombac, L. Sordelli, J.J. Delgado, X. Chen, G. Adami, P. Fornasiero, Nanostructured Cu/TiO2 photocatalysts for H2 production from ethanol and glycerol aqueous solutions, ChemCatChem 3 (2011) 574–577, https://doi.org/10.1002/cctc.201000289.
[87] C. Minero, A. Bedini, V. Maurino, Glycerol as a probe molecule to uncover oxidation mechanism in photocatalysis, Appl. Catal. B Environ. 128 (2012) 135–143, https://doi.org/10.1016/j.apcatb.2012.02.014.
[88] P. Ribao, M. Alexandra Esteves, V.R. Fernandes, M.J. Rivero, C.M. Rangel, I. Ortiz, Challenges arising from the use of TiO2/rGO/Pt photocatalysts to produce hydrogen from crude glycerol compared to synthetic glycerol, Int. J. Hydrog. Energy 44 (2019) 28494–28506, https://doi.org/10.1016/j.ijhydene.2018.09.148.
[89] M. Qureshi, K. Takanabe, Insights on measuring and reporting heterogeneous photocatalysis: efficiency definitions and setup examples, Chem. Mater. 29 (2017) 158–167, https://doi.org/10.1021/acs.chemmater.6b02907.
[90] M. Melchionna, P. Fornasiero, Updates on the roadmap for photocatalysis, ACS Catal. 10 (2020) 5493–5501, https://doi.org/10.1021/acscatal.0c01204.
[91] A. Beltram, I. Romero-Ocaña, J. Josè Delgado Jaen, T. Montini, P. Fornasiero, Photocatalytic valorization of ethanol and glycerol over TiO2 polymorphs for sustainable hydrogen production, Appl. Catal. A 518 (2016) 167–175, https://doi.org/10.1016/j.apcata.2015.09.022.
[92] T. Ohno, K. Sarukawa, K. Tokieda, M. Matsumura, Morphology of a TiO2 photocatalyst (Degussa, P-25) consisting of anatase and rutile crystalline phases, J. Catal. 203 (2001) 82–86, https://doi.org/10.1006/jcat.2001.3316.